Sensors and Actuators A 193 (2013) 112–120

Contents lists available at SciVerse ScienceDirect

Sensors and Actuators A: Physical

journal homepage: www.elsevier.com/locate/sna

Noninvasive current sensor for household appliances and compensation for installation variation

S.H. Cheng[a,b], S.F. Lin[a,*]

[a] Institute of Electrical Control Engineering, National Chiao Tung University, Taiwan, ROC
[b] Green Energy & Environment Research Laboratories, Industrial Technology Research Institute, Taiwan, ROC

ARTICLE INFO

Article history:
Received 16 September 2012
Received in revised form 11 January 2013
Accepted 11 January 2013
Available online 20 January 2013

Keywords:
Installation variation compensation
Energy management
Noninvasive current sensor

ABSTRACT

The lack of natural resources requires a more efficient use of energy. This study proposes a noninvasive coil current sensor for energy efficiency in the home. The proposed sensor is used to detect current in two-wire power cords used by household appliances. Moreover, the proposed sensor has no contact with the conductors in the power cords, ensuring a safe measurement process. Mathematical models and experiments are conducted to verify the characteristics and performance of the proposed device. In addition, this study develops relevant algorithms and the method for reducing installation variation. Using the developed algorithms, the measurement errors caused by an installation gap were reduced to less than 3%. The information provided by the current sensor supports home energy management systems and encourages energy-saving behaviors for every household member, resulting in an increasingly efficient energy usage.

1. Introduction

The lacks of natural resources and global warming have enabled the worldwide needs in improving energy efficiency. According to a recent Federal Energy Regulatory Commission report, the effective management and devising of electricity usage in residential areas is one of the most effective approaches for energy saving [1]. Moreover, the report indicated that residential demand response (DR) programs, which reduce the demand for electricity during shortages, could provide the largest potential reduction. Therefore, DR has become a technology trend in developing electricity monitoring systems for household energy management. Some scenarios of electrical energy monitoring and control systems in homes have been demonstrated [2–5], and all such scenarios emphasize energy information feedback, which causes behavioral changes in customers toward saving energy. The energy monitoring system can be simplified using current information alone because voltage fluctuations in homes are limited (for example, the voltage fluctuation in Taiwan is limited to ±10%). This study focuses on low-cost, easily installed, and reliable current sensors.

The principles in the current-sensing field include Ohm's law, Faraday's law of induction, magnetic field sensors, and the Faraday effect. Commercial current sensors, such as shunt resistors, Rogowski coils, current transformers, Hall sensors, magnetoresistance (MR) sensors, and fiber-optic current sensors (FOCSs), have been reported in previous studies [6–17]. Shunt resistors require contact with conducting paths and demonstrate large power losses in high-current applications. Rogowski coils must encircle the signal line separated from the neutral line in a two-wire appliance and produce electromotive forces that are proportional to the time derivative of the current in the conductor. Current transformers are similar to Rogowski coils, but with the disadvantages of magnetic hysteresis and saturation under high current. Hall sensors have large thermal drifts, offset voltages, and supply current requirements. MR sensors exhibit large thermal drift and high nonlinearity. FOCSs are expensive, extremely large, and barely adequate for high-current applications. Moreover, FOCSs are not suitable for use in household appliances, whose rms current ranges from 0 A to 15 A in two-wire power cords, without contacting conductors and separating wires.

A novel piezoelectric microelectromechanical system (MEMS) current sensor has also been proposed to sense electric current in two-wire power cords noninvasively [18,19]. The idea behind this current sensor includes a piezoelectric cantilever beam with a permanent magnet mounted at the free end. The cantilever beam is bent by magnetic force, which is proportional to the current in the power cords. Sensing signal is caused by the MEMS-scale cantilever beam and is thus influenced by vapor, so it requires a complex packaging process. Furthermore no schemes of calibration or compensation are addressed with this device. In the current study, another MEMS-based, cost-effective, flexible, inductive coil sensor is developed for a non-intrusive current detection to expedite the

* Corresponding author.
E-mail address: sflin@mail.nctu.edu.tw (S.F. Lin).

0924-4247/$ – see front matter © 2013 Elsevier B.V. All rights reserved.
http://dx.doi.org/10.1016/j.sna.2013.01.022

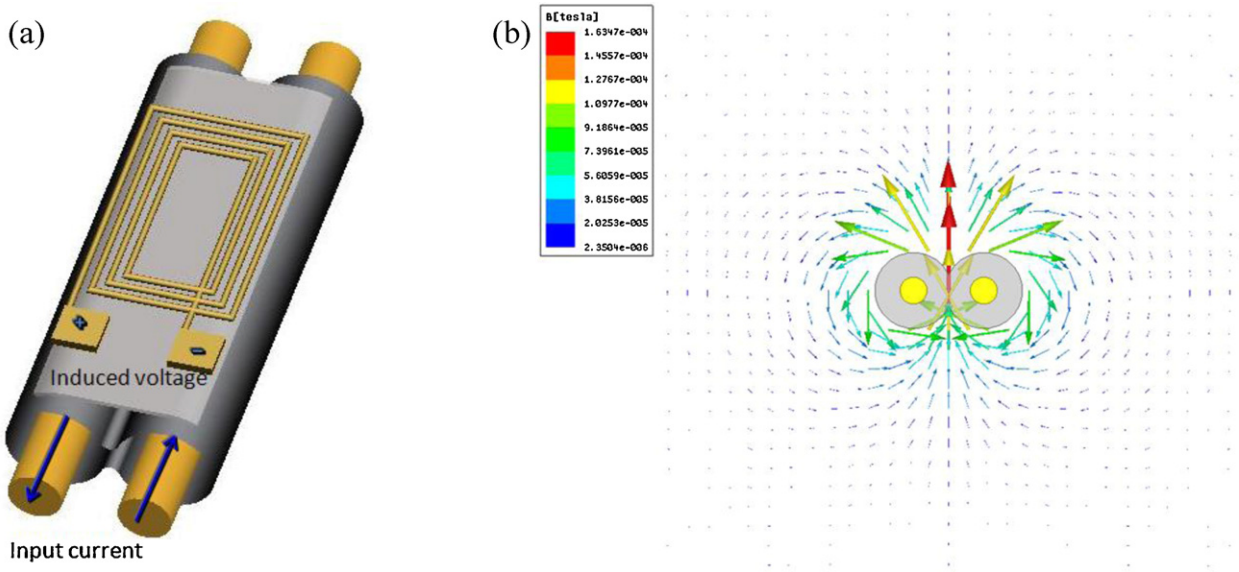

Fig. 1. (a) Proximity current monitor concept; and (b) simulation of magnetic flux distribution on a two-wire power cord.

application of ubiquitous energy awareness in the home, as shown in Fig. 1. Moreover, the manufacturing process and compensation methods for the different installation positions are also addressed.

The rest of this paper is organized as follows: Section 2 describes the inductive coil sensing mechanism and model; Section 3 presents the simulated results and proposes a compensating method for different installation positions; Section 4 presents the fabricating process and experimental results; and Section 5 draws the conclusions.

2. Device models

For a nonprofessional consumer, a current-monitoring instrument should be safe and convenient to use, and thus, noninvasive sensing is the optimal approach. The spatial magnetic field around a current-carrying conductor is proportional to the current in the conductor and uses the magnetic field to design the current sensor without making contact with the conducting paths. The use of coils according to Faraday's law is the simplest approach for measuring the spatial magnetic field. Fig. 1(a) shows the concept of the inductive coil current sensor.

According to Ampere's and Faraday's laws, the induced voltage generated by the input current can be described as follows:

$$V_{induced} = -\frac{d\phi}{dt} = -NA\frac{dB}{dt} = -\frac{NA\mu_0}{2\pi r}\frac{dI}{dt} \tag{1}$$

where Φ is the magnetic flux passing through the coil, A is the area encircled by the coil, N is the number of turns of the coil, B is the magnetic flux density, r is the radius from the center of the conductor to the sensor, I is the testing current, and μ_0 is the permeability of free space. The largest magnetic flux intensity on a two-wire power cord is located at the center of both conductors (Fig. 1(b)), which is where the inductive coil current sensor should be placed to maximize sensitivity.

Fig. 2(a) illustrates the geometry of a two-wire power cord and displays the detailed inductive coil model. Assuming that the current concentrated on a point and the radius of the point are close to zero, and then the model can be derived as follows:

$$\phi_n = \int \vec{B}_Z \cdot d\vec{A} = \frac{\mu_0 I \cos \omega t}{\pi} c_n \int_{a_n}^{b_n} \frac{x}{x^2 + g^2} dx \tag{2}$$

$$V_{induced} = -\sum_{n=1}^{N}\frac{d\phi_n}{dt} = \frac{\omega\mu_0 I \sin \omega t}{2\pi}\sum_{n=1}^{N} c_n \ln\left(\frac{b_n^2 + g^2}{a_n^2 + g^2}\right) \tag{3}$$

$$a_n = \frac{d}{2} - \frac{1}{2}[w_c - 2n \cdot w_d - 2(n-1) \cdot w_s] \tag{4}$$

$$b_n = \frac{d}{2} + \frac{1}{2}[w_c - 2n \cdot w_d - 2(n-1) \cdot w_s] \tag{5}$$

$$c_n = L - 2n \cdot w_d - 2(n-1) \cdot w_s \tag{6}$$

where Φ_n is the effective magnetic flux passing through the nth turn of the coils, ω is the angular frequency of the sinusoidal current, N is the total number of turns of the coils, w_d is the metal line width of the coils, w_s is the spacing between each turn, w_c is the outside diameter width of the coils, L is the outside diameter length of the coils, d is the distance between two central points of the conductors, g is the distance from the coils to the horizontal central shaft of both conductors, a_n is left boundary for each turn, b_n is right boundary for each turn and c_n is length inside the coil for each turn. Parameters a_n, b_n, and c_n are relative to the effective area for each turn. Based on this model, some key parameters are analyzed in the next section.

3. Simulation and analysis

This section discusses the effects of the parameters and compensates for the practical application to grasp the device characteristics.

3.1. Parameter effect

The characteristics of electronics components, as well as their installation differences, should be considered prior to their application. If the current sensor is not placed at the center of the power cord, then the effective magnetic flux passing through the coil will change. The parameter Δx referring to the point at $d/2$, which is the horizontal displacement, is introduced into the model. Total magnetic flux is build by superposition theorem. When coil is shifted to the right Δx, then two boundaries for right wire are $a_n + \Delta x$ and $b_n + \Delta x$ and two boundaries for left wire are $b_n - \Delta x$ and $a_n - \Delta x$. The definition of boundaries is from the close to the distant according to the position of the wire. The directions of current in right wire and left wire are opposite, so magnetic flux caused by right

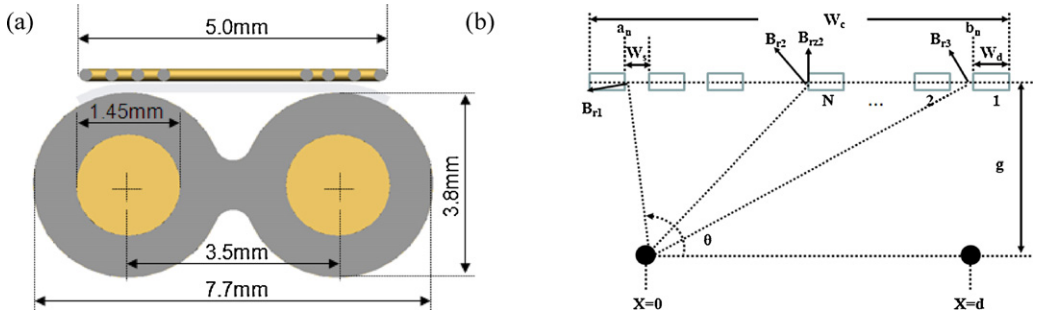

Fig. 2. (a) Geometry of a two-wire power cord; and (b) analysis of an inductive coil model.

wire and left wire are opposite, too. But they do not cancel each other out in the vertical direction at the central of the power cord (shown as Fig. 1b). Eq. (2) should be modified as follows:

$$\phi_n = \frac{\mu_0 I \cos \omega t}{2\pi} c_n \int_{a_n+\Delta x}^{b_n+\Delta x} \frac{x}{x^2+g^2} dx - \frac{\mu_0 I \cos \omega t}{2\pi} c_n \int_{b_n-\Delta x}^{a_n-\Delta x} \frac{x}{x^2+g^2} dx \quad (7)$$

Eqs. (3)–(7) show that w_d, w_s, w_c, L, d, g, and Δx affect the induced voltage. In fact, w_d, w_s, w_c, L, and d are manufacturer parameters that can be controlled precisely. Only g and Δx, which are caused by users, are evaluated in this study.

With regard to the power cord standards in Taiwan, the insulation thickness error is ±5% and g is the combined effect on the power cord thickness and installation variation in the vertical direction. The parameters w_d, w_s, w_c, L, d, and N are set to 30 μm, 30 μm, 5 mm, 10 mm, 3.5 mm, and 30 turns, respectively. As can be seen in Fig. 1(b), the magnetic flux density was largest at the center of the power cord. For simplification, the current sensor was assumed to be at the center of the power cord. Table 1 lists the variations in induced voltage with changing vertical distances and Fig. 3 shows the trend of gap effect, where the testing current is 1 A_{rms}. A 0.1 mm change in the vertical direction produced approximately 5% variation. Because g at 2.0 mm is a standard used for calculating the effect of gap variation, $Var.(g)$ is obtained by Eq. (8).

$$Var.(g) = \frac{V_{induced}(g) - V_{induced}(g=2.0)}{V_{induced}(g=2.0)} \times 100\% \quad (8)$$

For the effect of shift Δx, the parameter g is set to 2.0 mm and all the other parameters remain unchanged. Table 2 lists the horizontal shift effects and Fig. 4 shows the trend of shift effect. More than half of the magnetic flux in the vertical direction changed from up to down when the shift was greater than 3.2 mm, as shown in

Table 1
Gap effect.

g (mm)	$V_{induced}$ (μV)	*Var.* (%)
1.8	37.73	11.23
1.9	35.76	5.41
2.0	33.92	0
2.1	32.21	−5.05
2.2	30.61	−9.76
2.3	29.12	−14.15
2.4	27.72	−18.27
2.5	26.42	−22.12
2.6	25.19	−25.73
2.7	24.04	−29.12
2.8	22.97	−32.30
2.9	21.95	−35.29
3.0	21.00	−38.10

Installation gap is expected to be 0.1 mm, and 2.0 mm g is a standard used for calculating the gap change effect. *Var.* indicates the variation in comparison with the standard g.

Table 2
Shift effects.

Δx (mm)	V_{induce} (μV)	*Var.* (%)
0	33.92	0
0.4	32.94	−2.90
0.8	30.12	−11.19
1.2	25.86	−23.76
1.6	20.67	−39.08
2.0	15.06	−55.60
2.4	9.55	−71.86
2.8	4.53	−86.65
3.2	0.33	−99.04
3.6	−2.87	−108.47

Expected g is 2.0 mm and *Var.* indicates the variation in comparison with the no shift.

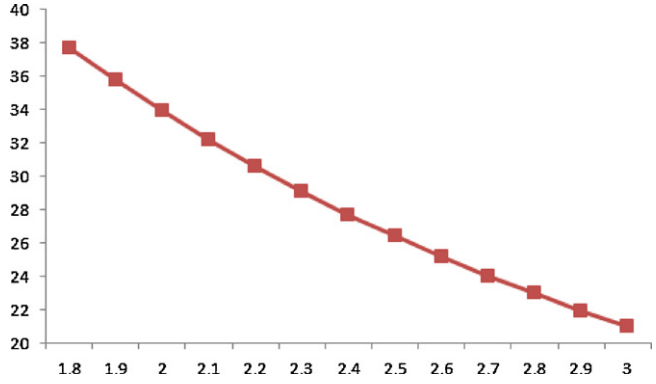

Fig. 3. The trend of gap effect.

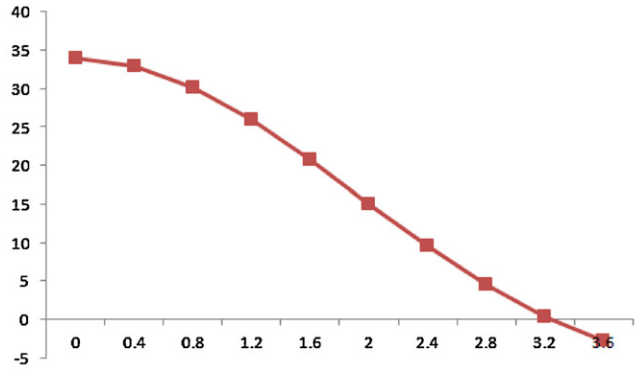

Fig. 4. The trend of shift effect.

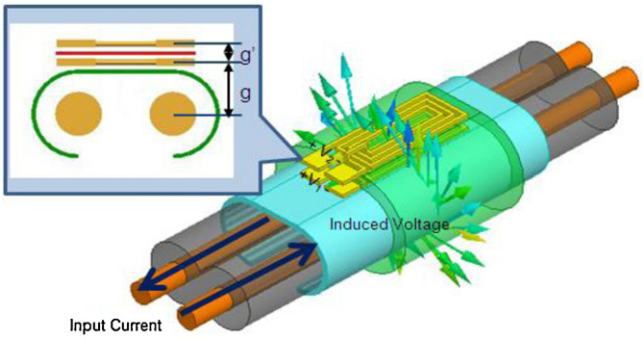

Fig. 5. Concept of calculating spacing g and test current *I* for the proximity current sensor.

Figs. 1(b) and 2(b). The induced voltage polarity changed with a variation of more than 100% and $Var.(\Delta x)$ is obtained by Eq. (9).

$$Var.(\Delta x) = \frac{V_{induced}(\Delta x) - V_{induced}(\Delta x = 0)}{V_{induced}(\Delta x = 0)} \times 100\% \quad (9)$$

Different installation gaps and shifts generate significant errors in the measurement results. Thus, installation gap variations and shifts should be compensated prior to implementation. A simple method to compensate for the different installation gaps automatically and shifts manually is discussed below.

3.2. Compensation for different installation positions

The current sensor is integrated into the power monitor system, and the measurement errors are calibrated using the standard current source in the final process. From a systematic perspective, changes in all aforementioned parameters are not serious issues. However, if the current sensor is a stand-alone product or if no standard current source is available to calibrate the measurement system, then the installation variation shifts and gaps should be overcome.

Fig. 5 shows the ideal solution for the gap variations in installation. According to Eq. (3), two equations are required to solve two unknown variables g and I that affect the induced voltage. Two-layer current sensors having two induced voltage values to solve the two unknown variables are designed with a fixed distance g' in the vertical direction. The simultaneous equations are expressed in Eq. (10), where coefficients K_{near} and K_{far} are introduced to express the differences between the ideal model and the real device, $Gain_{PCB}$ represents the sensing circuit gain, and V_{near} and V_{far} are the induced voltages of two current sensors.

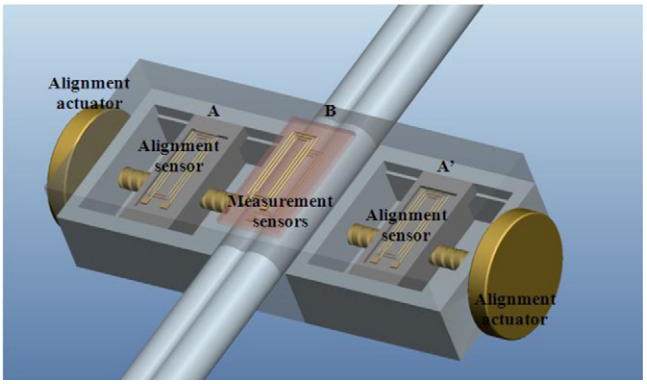

Fig. 7. Architecture of an alignment method.

$$V_{near} = K_{near} Gain_{PCB} \frac{\omega \mu_0 I \sin \omega t}{2\pi} \sum_{n=1}^{N} c_n \ln\left(\frac{b_n^2 + g^2}{a_n^2 + g^2}\right)$$
$$V_{far} = K_{far} Gain_{PCB} \frac{\omega \mu_0 I \sin \omega t}{2\pi} \sum_{n=1}^{N} c_n \ln\left(\frac{b_n^2 + (g+g')^2}{a^2 + (g+g')^2}\right) \quad (10)$$

Eq. (10), which contains natural logarithm and summation functions, can be solved using a look-up table by a general-purpose microprocessor. Using such method, a table containing the measurement system gains versus indices, relating to installation gaps, should be constructed. The steps for building this table by using a standard current source are as follows:

(1) Use Eq. (11) to obtain the indices ($index_g$);
(2) Use Eq. (12), where $I = 1$ is set at the beginning, to obtain measurement system gains ($Gain_{Measurement}$);
(3) Use Eq. (13) to build a measurement system gains versus indices table; and
(4) Use Eq. (14) to obtain an unknown current for implementation.

Indices versus measurement system gains is a one-to-one monotonic function, as shown in Fig. 6, and thus, a measurement system gain can be determined by an index. As can be seen in

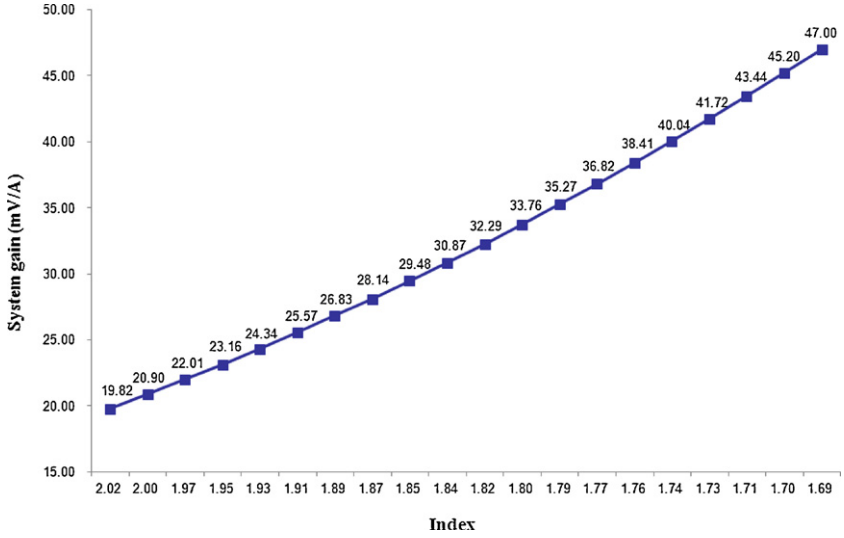

Fig. 6. Monotonic relationship of the indices and measurement system gains by simulation where testing current is 1 A_{rms} and gain of the read-out circuit is 66 dB.

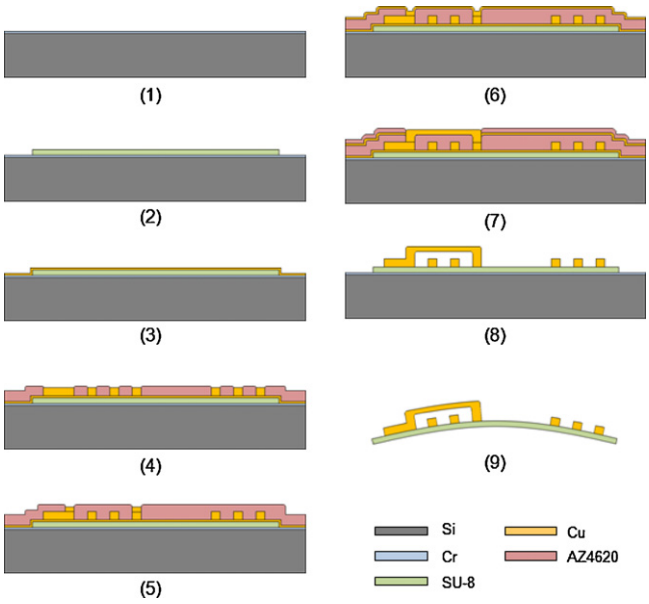

Fig. 8. Fabrication process flow of the flexible current sensor.

Table 1, approximately 5% error is generated per 0.1 mm increase in the installation gap (g) without compensation. A look-up table must be built per 0.1 mm to obtain measurement results with less than 5% errors.

$$\frac{V_{near}}{V_{far}} = \frac{K_{near}\sum_{n=1}^{N}\ln((b_n^2+g^2)/(a_n^2+g^2))}{K_{far}\sum_{n=1}^{N}\ln((b^2+(g+g')^2)/(a^2+(g+g')^2))} = index_g = f(g) \quad (11)$$

$$Gain_{Measuremert}(g) = \frac{I(I=1)}{V_{near}} = \frac{1}{k_{near}\frac{\omega\mu_0\sin\omega t}{2\pi}\sum_{n=1}^{N}c_n\ln((b_n^2+g^2)/(a_n^2+g^2))\times Gain_{PCB}} \quad (12)$$

$$Gain_{measuremert}(g) = f(index_g) \quad (13)$$

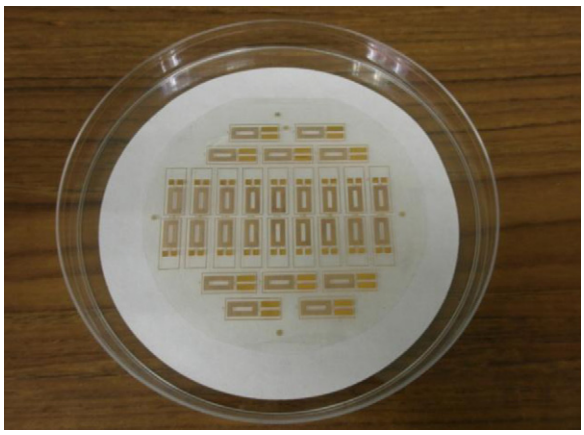

Fig. 9. Prototypes of the flexible current sensors.

$$I = V_{near}\times Gain_{measuremert}(g) = V_{near}\times f(index_g) \quad (14)$$

Second, the current sensor sensing result is also affected by a shift in the installation process. Two lateral inductive coils are designed to solve the horizontal shift problem. Fig. 7 illustrates the alignment method of the current sensor. To implement this method, a clamp with alignment lines which are pattern for four coils installing is design and position B is at the central of A and A′. The two alignment coils are stuck on the position A and A′, and the other two measurement coils are stuck on the upper and lower sides at the position B with a 1.5 mm bulkhead machining by a milling machine. The four coils are stuck by double-sided tapes. When signals of two alignment coils are not comparable, two alignment actuators are turned and made the power cord move right or left until signals of two alignment coils are comparable. Then the current sensor is positioned at the center of the power cord and the clamp makes measurement system be steadier.

Compensating for installation shifts is intuitive and without any issues, and thus, the experiments in the next section focus on compensating for installation gaps.

4. Fabrication and experimental verification

The flexible current sensor is fabricated using the MEMS process, which can be described as follows:

(1) A 150 nm thick sacrificial Cr layer is deposited onto a silicon substrate for the coil sensor release.

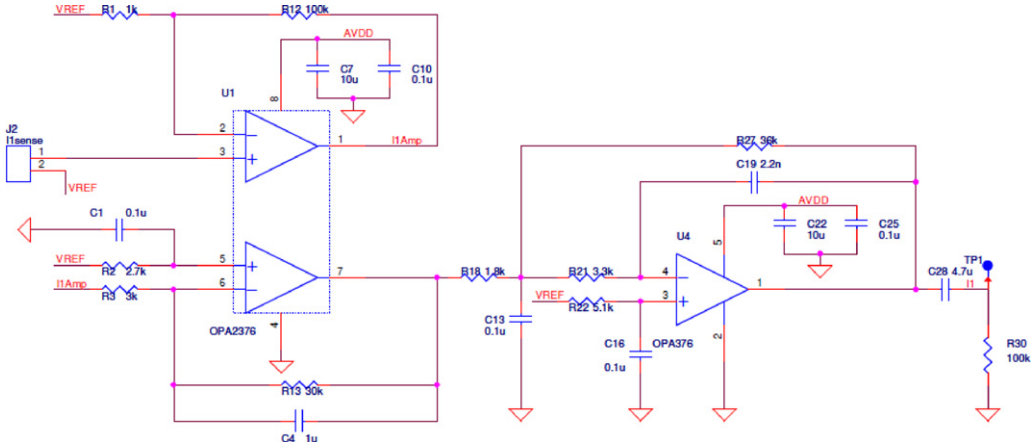

Fig. 10. Schematic diagram of a two-stage amplifier with a low-pass filter.

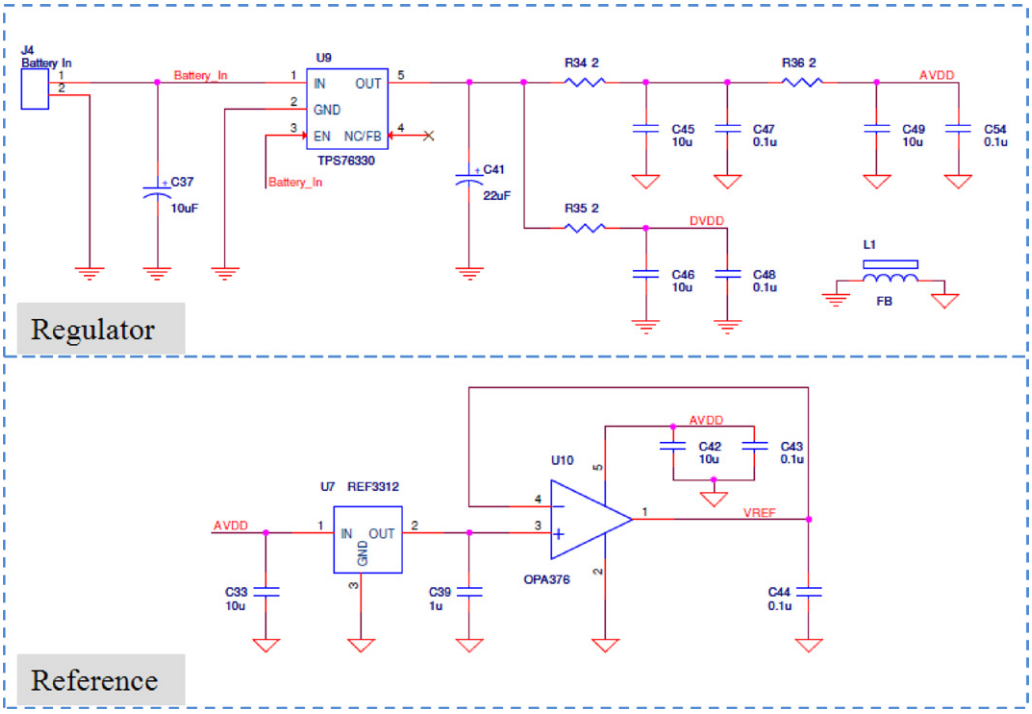

Fig. 11. Single power supply and reference voltage circuits.

(2) A 40 μm thick SU-8 photoresist is spin-coated and then patterned.
(3) A Ti (30 nm)/Cu (150 nm) adhesion/seed layer is deposited.
(4) A 7 μm thick AZ4620 photoresist is patterned on the adhesion/seed layer and used as a mold for a 5 μm thick electroplating Cu.
(5) A 5 μm thick photoresist is patterned to form via holes and then Cu is electroplated into holes.
(6) A 150 nm thick Cu seed layer is deposited.
(7) The substrate is coated with the patterned 7 μm thick AZ4620 photoresist and electroplated with a 5 μm thick Cu for the coil bridge fabrication.
(8) The substrate is dipped in acetone, Cu etchant, and buffered oxide etch (BOE) solution to remove the photoresist, seed layer, and adhesion layer, respectively.
(9) The flexible coil is released from the silicon substrate by dipping it in a Cr etchant (H_2O:HCl = 100:20) for the sacrificial layer removal (Figs. 8 and 9).

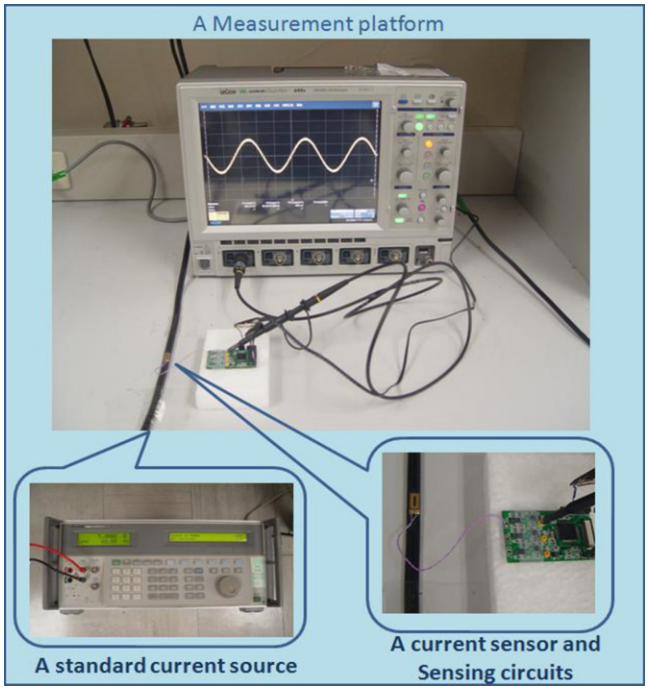

Fig. 12. Current-sensing system experiment platform at fixed position.

Based on the simulation, the induced voltage level is in μV, and the coils appear to be antennae that receive high-frequency noises. An amplifier and a filter should be designed for a practical application. Eq. (1) shows that the high-frequency signals are amplified because of the differential function, so an integrator is needed, too. This study provides a two-stage amplifier and an integrator,

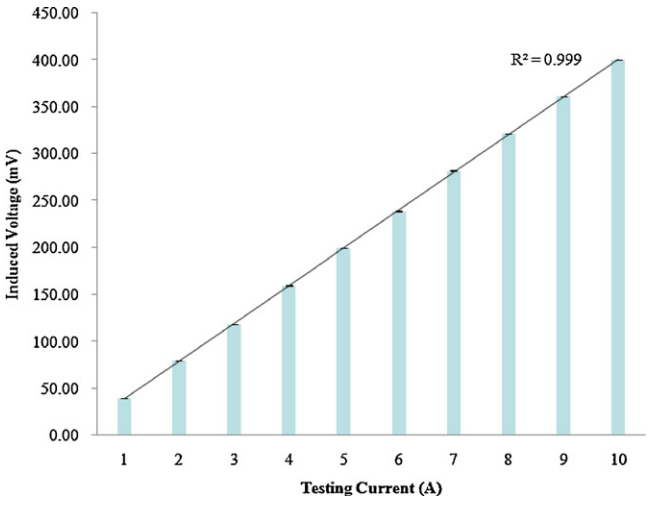

Fig. 13. Relationship of the testing currents and induced voltages of the inductive coil current sensor where error bars are made with standard deviations.

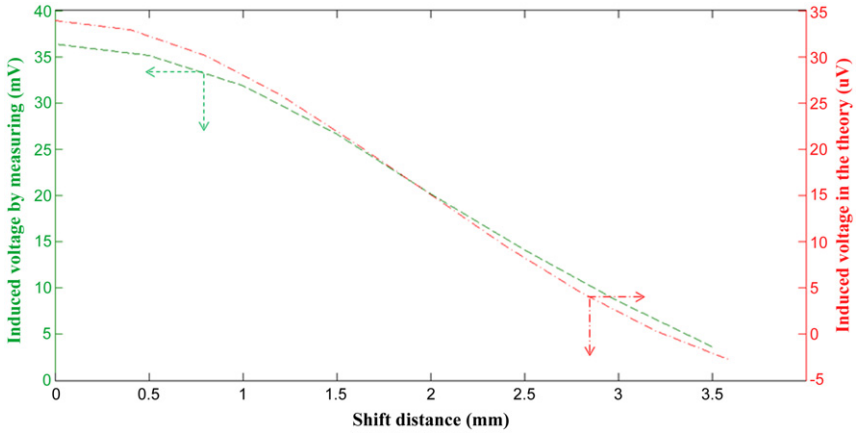

Fig. 14. Trends of shift effect between the theory and the experimental results.

as shown in Fig. 10. The first operational amplifier (op amp) provides amplification with a 26 dB gain. The second op amp functions as an integrator, and the third op amp provides amplification with a 26 dB gain. A low-pass filter (LPF) with multiple-feedback architecture and its transfer functions are expressed in Eq. (15). In this study, the LPF's cut-off frequency was set to 1 kHz with the consideration of the maximum harmonic, which does not exceed 15 orders of magnitude. The operational amplifier OPA376 operating on a single supply is used to implement the sensor nodes easily. The total harmonic distortion and the SNR of only 0.0007% ensure that the signal linearity is not affected. Power is supplied from a low-dropout regulator TPS76330, whose output is 3.0 V. A 1.2 V reference voltage set by REF3312 is designed to satisfy dipolar input signals because the operational amplifier only has a single supply, as shown in Fig. 11.

$$T_{LPF}(s) = \frac{R_{27}/R_{18}}{1 + w_c C_{19}(R_{21} + R_{27} + (R_{21} \times R_{27}/R_{18})) \cdot s + w_c^2 c_{19} c_{13} R_{21} R_{27} s^2} \quad (15)$$

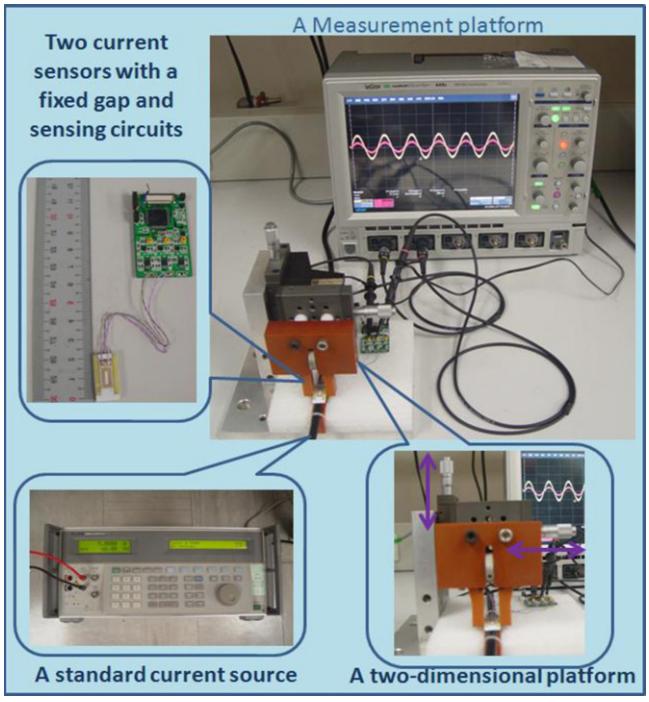

Fig. 15. Experimental platform for verifying the compensation algorithm.

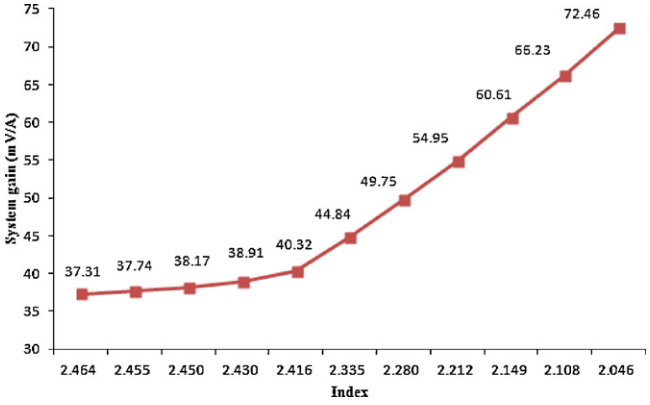

Fig. 16. Relationship of measurement system gains and indices.

Fig. 12 shows the testing system, which includes a current source, an oscilloscope, a two-wire power cord, a flexible current sensor, and sensing circuits. The experimental data were obtained using an oscilloscope, and the measurement characteristic of the coil current sensor was found to be linear, as shown in Fig. 13.

The experiment demonstrated a linearity characteristic, which makes the coil current sensor adequate for use as a sensing component in a power monitor system. The sensor can be calibrated using a standard current source because of its linearity.

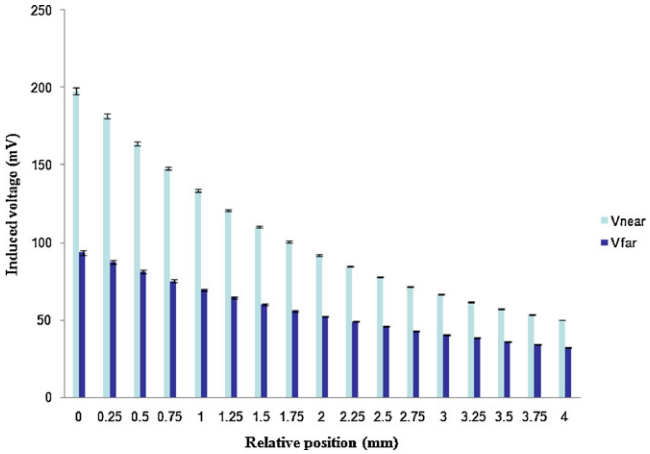

Fig. 17. A testing of the reproducibility where error bars are made with standard deviations and testing current is 5 A_{rms}.

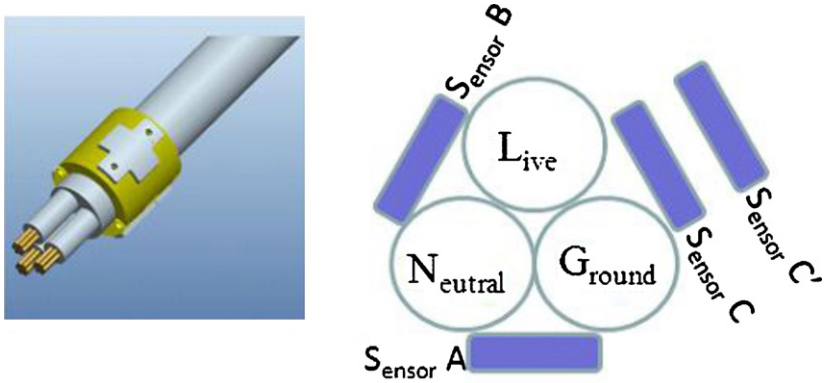

Fig. 18. The scheme of current measurement for three-wire power cords.

Table 3
Verification of the compensation algorithm at different gaps.

g (mm)	Induced voltage of the near coil (mV)	Index	System gain (A/mV)	Calculated current (A)	Error (%)
Δ + 0.1	385.23	2.4534	37.74	10.28	2.8
Δ + 0.2	381.11	2.4588	37.59	10.13	1.3
Δ + 0.3	376.39	2.4501	38.17	10.16	1.6
Δ + 0.4	370.13	2.4441	38.31	10.03	0.3
Δ + 0.5	356.90	2.4317	38.76	9.78	−2.2
Δ + 0.6	319.88	2.3472	44.05	9.97	−0.3
Δ + 0.7	286.54	2.2660	50.76	10.29	2.9
Δ + 0.8	261.68	2.2269	53.76	9.95	−0.5
Δ + 0.9	237.08	2.1600	59.52	9.98	−0.2
Δ + 1.0	216.48	2.1089	66.23	10.14	1.4
Δ + 1.1	198.41	2.0659	70.42	9.88	−1.2

Δ is the distance between the center of a conductor and the coil closest to the power cord's start. The error is calculated by (calculated current − testing current)/testing current × 100%.

Additional functions must be built to overcome the installation differences in a stand-alone product without a standard current source. As described in Section 3, the shift variation is overcome by the user, and thus, this study focuses on compensating the variations in g. Following experiments are based on Eq. (2), so let us verify Eq. (7) with measuring data and have an ending for shift effect. Fig. 14 shows trends of shift effect between the theory and the experimental results and the trends are consistent, in general.

Compensating for gap, two current sensors are proposed to solve the problem. Fig. 15 shows the experimental platform, which includes a current source, an oscilloscope, a two-wire power cord, sensing circuits, two flexible current sensors with 1.5 mm thick plastic, and a two-dimensional moveable platform. The two-dimensional platform was moved horizontally to maximize the induced voltage of the current sensors, and then moved vertically to obtain the measurement system gains versus indices. All data was obtained using an oscilloscope. Fig. 16 shows the measurement system gains versus indices, where the testing current was set at 5 A_{rms}.

The two-wire power cord was taken away and then placed in the platform again. The two-dimensional platform was then moved horizontally to maximize the induced voltage of the current sensors. To verify the compensation method for the installation gap, the 10 A_{rms} testing current was connected to the power cord and the platform was moved vertically to obtain the indices, which are functions of g. The index was calculated per 0.1 mm distance away from the power cord. Table 3 shows the relationship of the measured current with the different gaps at 10 A_{rms} testing current, which was calculated based on the measurement system gains versus indices table shown in Fig. 13 and by using linear interpolation. The results show that the errors do not over 5%, and the algorithm is useful to compensate gap variations.

An investigation of reproducibility is studied in this paper to judge whether the current sensing device is applied. To study in the reproducibility which is focused on vertical, we move two-dimensional platform from bottom to top and record the signals of two coils at three different days. The results are shown in Fig. 17 and the devices are with good reproducibility.

Finally, a circular clamp with four coils is designed to expand the applications for signal-phase three-wire power cords. Rotating the circular clamp until the induced voltages of sensor A and sensor B are equal. And then sensor C and sensor C′ are at the middle of the live and neutral lines (shown as Fig. 18). Then the measurement and compensation are similar to two-wire power cords.

5. Conclusion

This study described the feasibility of noninvasive current sensing for two-wire power cords and solved the installation variation without using a standard current source for implementations. The proposed device supports home energy management systems and encourages energy-saving behaviors for every household member, resulting in an increasingly efficient energy usage.

Future studies can focus on new algorithms that can combine installation gap and shift compensation automatically and on the manufacturing method of inductive coil current sensors. A multilayered coil current sensor should be designed to enhance induced voltage because induced voltage is proportional to the number of turns of the coils.

Acknowledgment

This work was supported in part by the Bureau of Energy, Ministry of Economic Affairs, Taiwan, ROC., under contract No. 101-D0309.

References

[1] E.A. Arens, D. Auslander, D. Culler, C. Federspiel, C. Huizenga, J. Rabaey, P. Wright, P. White, Demand Response Enabling Technology Development, UC Berkeley, Center for the Built Environment, 2006, Available from: http://www.escholarship.org/uc/item/0971h43j

[2] H.C. Sun, Y.C. Huang, Optimization of power scheduling for energy management in smart homes, Procedia Engineering 38 (2012) 1822–1827.

[3] Y.T. Chen, J.K. Hwang, A reliable energy information system for promoting voluntary energy conservation benefits, IEEE Transactions on Power Delivery 21 (1) (2006) 102–107.

[4] D.M. Han, J.H. Lim, Design and implementation of smart home energy management systems based on zigbee, IEEE Transactions on Consumer Electronics 56 (3) (2010) 1417–1425.

[5] N.G. Dlamini, F. Cromieres, Implementing peak load reduction algorithms for household electrical appliances, Energy Policy 44 (2012) 280–290.

[6] S. Ziegler, R.C. Woodward, H.H.-C. Iu, L.J. Borle, Current sensing techniques: a review, IEEE Sensors Journal 9 (4) (2009) 354–376.

[7] B. Voljc, M. Lindic, R. Lapuh, Direct measurement of AC current by measuring the voltage drop on the coaxial current shunt, IEEE Transactions on Instrumentation and Measurement 58 (4) (2009) 863–867.

[8] W.F. Ray, C.R. Hewson, High performance Rogowski current transducers, in: Proceedings of IEEE Industrial Application Conference, Rome, Italy, 2000, pp. 3083–3090.

[9] M. Chiampi, G. Crotti, A. Morando, Evaluation of flexible Rogowski coil performances in power frequency applications, IEEE Transactions on Instrumentation and Measurement 60 (3) (2011) 854–862.

[10] M. Yahyavi, F. Brojeni, M. Vaziri, Basic Theory, Practical considerations in a current transformer, in: Proceedings of PENGM 2007, June 2007, pp. 1–8.

[11] A. Cataliotti, D. Di Cara, A.E. Emanuel, S. Nuccio, Improvement of Hall effect current transducer metrological performances in the presence of harmonic distortion, IEEE Transactions on Instrumentation and Measurement 59 (5) (2010) 1091–1097.

[12] Y. Wei, Z. Yue, M. Anheuser, A residual current measurement method with a combination of MR and Hall effect sensors, in: Proceedings of AMPS, Aachen, Germany, 2010, pp. 27–30.

[13] P. Mlejnek, M. Vopálenský, P. Ripka, AMR current measurement device, Sensors and Actuators A Physical 141 (2) (2008) 649–653.

[14] P. Ripka, M. Janosek, Advances in magnetic field sensors, IEEE Sensors Journal 10 (6) (2010) 1108–1116.

[15] K.T.V. Grattan, T. Sun, Fiber optic sensor technology: an overview, Sensors and Actuators A Physical 82 (1–3) (2000) 40–61.

[16] S.J. Petricevic, Z. Stojkovic, J.B. Radunovic, Practical application of fiber-optic current sensor in power system harmonic measurement, IEEE Transactions on Instrumentation and Measurement 55 (3) (2006) 923–930.

[17] P. Niewczas, J.R. McDonald, Advanced optical sensors for power and energy systems applications, IEEE Instrumentation and Measurement Magazine 10 (1) (2007) 18–28.

[18] E.S. Leland, P.K. Wright, R.M. White, Design of a MEMS passive, proximity-based AC electric current sensor for residential and commercial loads, in: Proceedings of Power MEMS, Freiburg, Germany, 2007, pp. 77–80.

[19] E.S. Leland, C.T. Sherman, P. Minor, P.K. Wright, R.M. White, A new MEMS sensor for AC electric current, in: Proceedings of IEEE Sensors, 2010, pp. 1177–1182.

Biographies

Hsih-Hsien Cheng was born in Chiayi, Taiwan, ROC in 1975. He received his B.S. degree in control engineering from Feng Chia University, Taichung, Taiwan in 1998 and his M.S. degree in electrical engineering from National Sun Yat-sen University, Kaohsiung, Taiwan in 2000. He is currently a Ph.D. candidate at National Chiao Tung University, Hsinchu, Taiwan and is also a research staff with the Green Energy & Environment Research Laboratories, Industrial Technology Research Institute, Chutung, Taiwan. His current research interests include power electronics, power measurement, neural networks, fuzzy theory, and wireless sensor networks.

Sheng-Fuu Lin was born in Tainan, Taiwan, ROC in 1954. He received his B.S. and M.S. degrees in mathematics from National Taiwan Normal University in 1976 and 1979, respectively, his M.S. degree in computer science from the University of Maryland, College Park, in 1985, and his Ph.D. degree in electrical engineering from the University of Illinois, Champaign, in 1988. Since 1988, he has been with the faculty of the Department of Electrical Engineering at National Chiao Tung University, Hsinchu, Taiwan, where he is currently a professor. His research interests include image processing, image recognition, fuzzy theory, neural networks, automatic target recognition, intelligent system design, and computer vision.